Journal of Materials Chemistry A

COMMUNICATION

View Article Online
View Journal

Cite this: DOI: 10.1039/c5ta09530a

Received 24th November 2015
Accepted 9th February 2016

DOI: 10.1039/c5ta09530a

www.rsc.org/MaterialsA

Oxygen evolution reaction electrocatalysis on $SrIrO_3$ grown using molecular beam epitaxy†

Runbang Tang,‡[a] Yuefeng Nie,‡[ab] Jason K. Kawasaki,‡[bc] Ding-Yuan Kuo,[a] Guido Petretto,[d] Geoffroy Hautier,[d] Gian-Marco Rignanese,[d] Kyle M. Shen,[bc] Darrell G. Schlom[ac] and Jin Suntivich*[ac]

Electrochemical generation of oxygen *via* the oxygen evolution reaction (OER) is a key enabling step for many air-breathing electrochemical energy storage devices. IrO_2 (Ir^{4+}: $5d^5$) ranks among the most active known OER catalysts. However, it is unclear how the environment of the Ir^{4+} oxygen-coordination octahedra affects the OER electrocatalysis. Herein, we present the OER kinetics on a single-crystal, epitaxial $SrIrO_3(100)_p$ perovskite oxide synthesized using molecular-beam epitaxy on a $DyScO_3(110)$ substrate. We find that by switching the host structure of the Ir^{4+} oxygen-coordination octahedra from corner- and edge-sharing rutile (IrO_2) to purely corner-sharing perovskite ($SrIrO_3$), the OER activity increases by more than an order of magnitude. We explain our finding with the correlated, semimetal electronic structure of $SrIrO_3$; our density functional theory calculations reveal that the adsorption energetics on $SrIrO_3$ depends sensitively on the electron–electron interaction, whereas for IrO_2, it depends rather weakly. This finding suggests the importance of correlations on the OER and the design of future transition metal oxide electrocatalysts.

The kinetics of the oxygen evolution reaction (OER, in alkaline: $4OH^- \rightarrow O_2 + 2H_2O + 4e^-$) is central to the efficiency of many air-breathing electrochemical energy storage systems, including solar- and electricity-driven electrolysis[1–3] and rechargeable metal–air batteries.[4–6] In an effort to find superior materials as OER catalysts to decrease the activation overpotential, Trasatti has surveyed the OER kinetics over a large number of transition metal oxides[7] and identified IrO_2 and RuO_2 as the most active binary OER electrocatalysts. Decades later, using *ab initio* calculations, Nørskov and Rossmeisl have suggested that the high OER activities of these precious-metal oxides are due to the stable formations of the intermediates during the OER.[8–10] Using the scaling relation, they also established the surface oxygen binding as a descriptor to the OER activity. Inspired by this finding, intensive efforts have been spent on identifying strategies for controlling the surface oxygen interactions by using, for example, transition metal substitutions,[11–13] structural engineering,[14,15] and support interactions.[16–18] Although these efforts have led to successful developments of new OER electrocatalysts, the studies have largely focused on polydisperse-oxide materials. The reliance on the polydisperse materials complicates the process of connecting the surface structure with the electrochemical mechanism as there can be different terminations, structural defects, or even multiple phases present within the same catalytic material.[19,20]

In the past few decades, advances in deposition technologies and substrate availabilities have enabled the growth of single-crystal transition metal oxide films with high structural perfection. These advances have driven recent work in elucidating the electrochemistry on single-crystal transition metal oxides and allowed for a very precise determination of the electrokinetics.[20] Still, very few well-defined, single-crystal 5d transition metal oxides surfaces, notably IrO_2, have been studied as OER catalysts.[20,21] Herein, we report the OER kinetics on a well-defined, single-crystal 5d perovskite-oxide $SrIrO_3$ catalyst that was synthesized using molecular-beam epitaxy (MBE). We find that the OER activity of the $SrIrO_3$ is more than an order of magnitude higher than IrO_2, despite both $SrIrO_3$ and IrO_2 sharing the same active $Ir^{4+}O_6$ octahedral unit. Our density function theory (DFT) calculations assuming a previously reported OER pathway[8–10] suggest the OOH* formation as the most energy-intensive intermediate on $SrIrO_3$ during the OER. We further find that the calculated energetics depends on the Hubbard U, which reflects the correlated nature of $SrIrO_3$. Although this correlation renders the process of assigning the

[a]Department of Materials Science and Engineering, Cornell University, Ithaca, New York 14853, USA. E-mail: jsuntivich@cornell.edu

[b]Laboratory of Atomic and Solid State Physics, Department of Physics, Cornell University, Ithaca, New York 14853, USA

[c]Kavli Institute at Cornell for Nanoscale Science, Cornell University, Ithaca, New York 14853, USA

[d]Institute of Condensed Matter and Nanosciences (IMCN), Université Catholique de Louvain, Louvain-la-Neuve 1348, Belgium

† Electronic supplementary information (ESI) available. See DOI: 10.1039/c5ta09530a

‡ Equal contributions.

energetics less straightforward, as we will discuss later, we see this phenomenon as an opportunity for the design of future transition metal oxide electrocatalysts.

$SrIrO_3$ has received widespread attention as a material with a delicate balance between the spin–orbit interaction, the Coulomb interaction and the 5d electron delocalization.[22,23] The perovskite phase of $SrIrO_3$ is metastable by nature; realizing the perovskite phase of $SrIrO_3$ as opposed to the hexagonal 6H–$BaTiO_3$ phase requires a high-temperature, high-pressure synthesis condition.[24,25] We have recently reported the growth of single-crystal $SrIrO_3$ thin films with high structural perfection using MBE with low-pressure ozone as an oxidant.[26,27] Through angle-resolved photoemission spectroscopy (ARPES), we have shown that $SrIrO_3$ is a narrow-band semimetal as a result of the spin–orbit interaction that breaks the degeneracy of the t_{2g} orbitals into the $J_{eff} = 1/2$ and 3/2 states.[27] This bandwidth narrowing, induced by the spin–orbit interaction, the electron–electron interaction and the octahedra rotation, turns $SrIrO_3$ into a correlated semimetal.[23] From the electrocatalysis perspective, $SrIrO_3$ is an interesting 5d transition metal oxide compound to examine, especially in comparison to IrO_2. Notably, although both share a similar electronic configuration (Ir^{4+}: $5d^5$), the semimetal $SrIrO_3$ perovskite exhibits moderate electronic correlations, in comparison to the rutile IrO_2, which is a weakly correlated metallic oxide.[28–30] Many theoretical investigations had discussed the possibility of using crystal structure[31,32] and electron–electron interaction to tune the activity.[33,34] Examining the OER activity of $SrIrO_3$ in comparison to IrO_2 can provide insights into whether the structural difference (perovskite *vs.* rutile) and the resulting electron–electron interaction change can affect the OER activity, the result of which can open up the study of a new structure–activity relationship beyond a local crystal-field octahedral manifold commonly used.[3,35]

We grew $SrIrO_3(100)_p$ (subscript p denoting the pseudocubic orientation) films on single-crystal $DyScO_3(110)$ substrates using the procedure reported previously.[27] Fig. 1 shows a θ–2θ X-ray diffraction scan of a $SrIrO_3(100)_p$ film (40 formula-units thick). All the peaks can be assigned to the $SrIrO_3$ film and the $DyScO_3$ substrate. Reflection high-energy electron diffraction (RHEED), measured during the $SrIrO_3$ growth, shows a sharp, streaky pattern, consistent with a growth of a smooth $SrIrO_3(100)_p$ single-crystal film (see ESI†). This in combination with the extensive structural (synchrotron X-ray diffraction, transmission electron microscopy, low-energy electron diffraction) and electronic characterizations (measurement of Fermi surface by ARPES) shown in ref. 27 demonstrates the high quality of the $SrIrO_3$ single-crystal film.

In Fig. 2, we show the cyclic voltammogram of $SrIrO_3$ in 0.1 M KOH. The presence of a reversible peak near 0.6 V *vs.* reversible hydrogen electrode (RHE) is notable; this peak does not appear in the rutile IrO_2 in either poly-crystalline, (100)-, (110)-oriented,[20] or in amorphous films.[36] Nonetheless, a similar peak appears in a hydrated, amorphous iridium oxide, albeit occurring at a slightly different potential, where it is conventionally assigned as the Ir^{III}/Ir^{IV} redox.[37,38] Integrating the charge underneath the CV curve of $SrIrO_3$ (from Fig. 2) reveals that the electrochemical current is consistent with a surface redox process (215 $\mu C\ cm^{-2}$ or $\sim 2.1e^-$ per surface Ir on the $SrIrO_3(100)_p$ surface). In comparison, the resulting integrated charge density of the hydrated iridate film, where the electrochemical process can occur inside the bulk material, is significantly larger (more than tens of $mC\ cm^{-2}$).[38–40] Considering that the integrated charge of $SrIrO_3$ ($2.1e^-$ per surface Ir) is already an overestimation as the CV in Fig. 2 likely contains more than one redox peak and also the double-layer capacitance – we believe that only the top layer of $SrIrO_3$ participates in the electrochemical process and is different from the bulk-active electrocatalytic oxides.[41] Post-electrochemistry X-ray diffraction of the oxide sample and inductively coupled plasma-mass spectrometry (ICP-MS) of the electrolyte support the assignment that only the surface layer participates in electrochemistry (see ESI†).

To further reveal the origin of the redox peak, we compare the cyclic voltammetry (CV) of $SrIrO_3$ in LiOH, NaOH and KOH

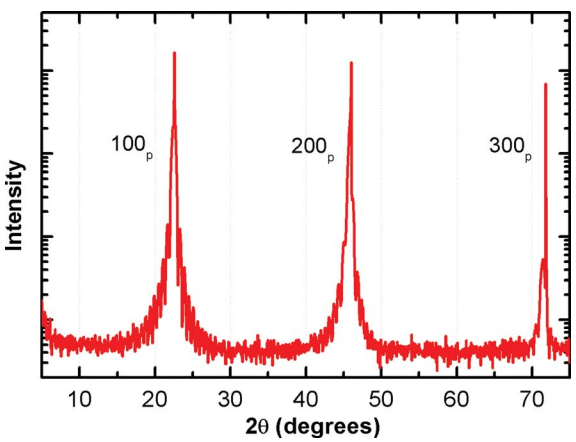

Fig. 1 Exemplary X-ray diffraction (θ–2θ scan) of the $SrIrO_3$ film (40 formula-units thick) grown on $DyScO_3(110)$. The pseudocubic reflections of $SrIrO_3$ (denoted as $L00_p$) confirm that the film is single phase with a $SrIrO_3(100)_p$ surface plane.

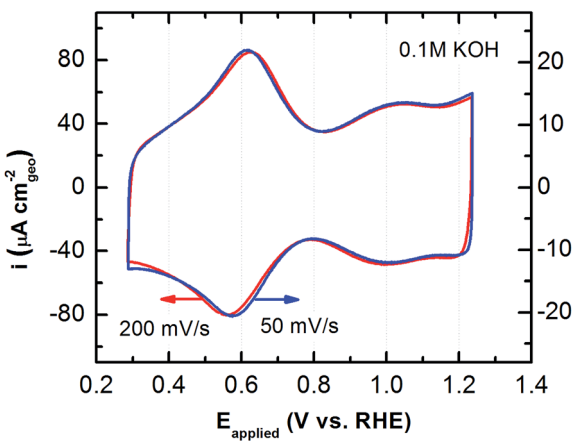

Fig. 2 Cyclic voltammograms of $SrIrO_3(100)_p/DyScO_3(110)$ film (40 formula-units thick) in Ar-saturated 0.1 M KOH at 50 mV s^{-1} and 200 mV s^{-1} scan rates.

(see ESI†). We observed no noticeable difference in all three electrolytes. This observation suggests that the cation does not participate in the redox peak at 0.6 V *vs.* RHE either directly or indirectly.[42,43] Therefore we assign this redox peak and the nearby feature to the anion-related reaction, specifically the hydroxide ($OH^- \rightarrow OH^* + e^-$) and the oxide electro-adsorption ($OH^* + OH^- \rightarrow O^* + H_2O + e^-$) on coordinatively undersaturated Ir sites. This assignment is in agreement with the observed charge density and the DFT calculation, which suggests that the electro-adsorptions of OH* and O* occur below 1.23 V *vs.* RHE, as is discussed in more detail below.

We further compare the CV of $SrIrO_3$ in a series of alkaline pH (see ESI†). We observe that the redox peak maintains the reversibility but shifts to higher electrochemical potentials (with respect to RHE) with acidic pH. Koper *et al.* have suggested that the origin of the pH dependence of the surface adsorption peak (with respect to RHE) can be from the mixed proton–electron/electron transfer nature of the surface electro-adsorption.[44,45] This scenario could happen for $SrIrO_3$, and hence an anomalous pH dependence. Alternatively, the shift of the redox peak could stem from the dependence of the nearest–neighbor interactions as a result of the pH shift or the surface reconstruction. In comparison to known surfaces with pH-dependent voltammetry, the observed shift in the redox peak with pH moves in the same direction as the hydrated iridium oxide but, interestingly, in the opposite direction as the hydrogen electro-adsorptions on Pt, which systematically shift to higher electrochemical potentials with increasing pH.[44–46] We emphasize that the exact origin of the pH dependence is still speculative; further *in situ* surface spectroscopy is essential to unravel the interaction at the $SrIrO_3$-electrolyte interface.

The OER kinetics for $SrIrO_3$ in 0.1 M KOH is shown in Fig. 3a. Assuming that the roughness factor (cm_{ox}^2/cm_{geo}^2) is ~1,[20,47] the OER kinetics for $SrIrO_3(100)_p$ is at least an order of magnitude higher than our $IrO_2(110)$ reference catalyst (Fig. 3b). Our $IrO_2(110)$ reference catalyst was grown on a single-crystal $TiO_2(110)$ substrate by MBE and has comparable OER activity to prior work[20] (see ESI† for the structural characterization of the IrO_2 film). We observe that the OER on $SrIrO_3$ exhibits a lower Tafel slope (~40 mV/decade, extracted from the low current density regime, <0.5 mA cm^{-2}, to minimize artifacts from the electrolyte-resistance correction) than rutile IrO_2 (~60 mV per decade).[20,48] In the Butler–Volmer kinetics expression, this Tafel slope translates to an anodic transfer coefficient (α) of 1.5, which indicates a potential-dependent surface coverage[49] or the possibility of a multi-electron pre-equilibrium.[50] To understand the OER electrocatalysis on $SrIrO_3$, we apply DFT calculations to examine the surface energetics of $SrIrO_3$. We follow the methodology developed by Nørskov and co-workers using a computational hydrogen electrode to estimate the intermediate energy of each of the proton-coupled electron transfer steps as a function of electrochemical potential.[8] We use the three intermediates (O*, OH* and OOH*) commonly assumed. Fig. 4a shows the calculated O*, OH* and OOH* energetics on $SrIrO_3$ and IrO_2 slabs (see ESI† for the calculation details). Our DFT calculations suggest that both OH* and O* formations on $SrIrO_3$ are favorable below 1.23 V *vs.* RHE, which provide support for the redox peak assignments discussed earlier. Our calculation reveals that $SrIrO_3$ requires the highest overpotential at the OOH* formation ($O^* + H_2O \rightarrow OOH^* + H^+ + e^-$).

While our DFT calculations support the OOH* formation as the potential-limiting step for the OER on $SrIrO_3$, we caution that we do not have evidence to support that the used OER mechanism is appropriate. In addition, there is a question of whether the DFT calculation accurately captures the surface energetics at the $SrIrO_3$–electrolyte interface. In an effort to demonstrate this complexity, we compare the O*, OH*, OOH* intermediate energies on $SrIrO_3$ and IrO_2 surfaces. As shown in Fig. 4, we point out the first challenge in this model; our DFT calculation suggests that IrO_2 requires less overpotential to form OOH* than $SrIrO_3$. Since the OOH* formation is the potential-limiting step for both $SrIrO_3$ and IrO_2 surfaces, the DFT calculations suggest that IrO_2 should possess superior OER kinetics than $SrIrO_3$. The prediction, however, that IrO_2 possesses superior OER kinetics than $SrIrO_3$ due to the OOH* formation energy is opposite from our experimental result.

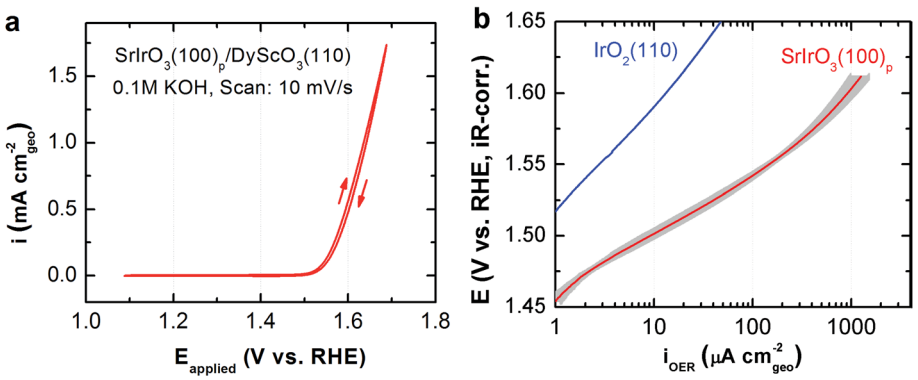

Fig. 3 (a) Cyclic voltammogram of $SrIrO_3(100)_p$ in O_2-saturated 0.1 M KOH at 10 mV s^{-1} (b) A Tafel plot of the OER kinetics of $SrIrO_3(100)_p$ and $IrO_2(110)$ films. The shaded area represents the standard deviation for three independent measurements.

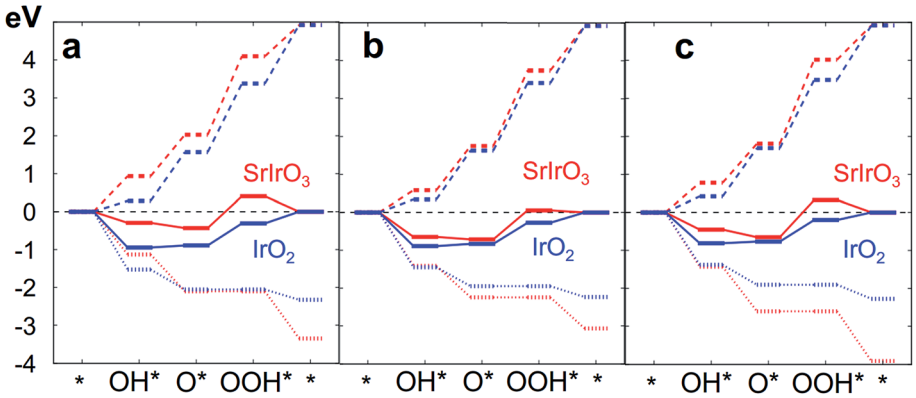

Fig. 4 Calculated free energies of the OER intermediates for IrO_2 and $SrIrO_3$: solid line at 1.23 V *vs.* RHE, dashed line at 0 V *vs.* RHE, dotted line for the minimum potential where the thermodynamic overpotentials are downhill. All calculations use GGA-RPBE (see ESI†) with (a) $U = 0$ eV, (b) $U = 1$ eV and (c) $U = 2$ eV.

The disagreement in the activity ordering could come from the difficulty in accurately predicting the surface energetics of correlated oxides such as $SrIrO_3$. We demonstrate this point by examining how O*, OH*, OOH* adsorption energetics can depend on the Hubbard term U (Fig. 4 and ESI†). This correction is introduced to heal the self-interaction error of the standard DFT approach.[51] While this is known to be a very effective correction for strongly correlated materials containing 3d transition metals,[33,52] its contribution may be more subtle when more delocalized 5d electrons are involved.[27]

Our calculation reveals that the adsorption energetics for $SrIrO_3$ depends sensitively on U, whereas for IrO_2, it does not. This specific behavior for $SrIrO_3$ can be related to the spin–orbit coupling effect, which localizes the 5d electrons and reduces the frontier bandwidth ($J_{\mathrm{eff}} = 1/2$) to a value comparable to U. As a result, $SrIrO_3$ becomes semi-metallic and sensitive to the partial charge change during the adsorption. Hence, the U correction can substantially affect the adsorption energetics on $SrIrO_3$. IrO_2, on the other hand, is metallic and therefore is insensitive. This is a rather interesting observation given that the Ir–O distance only differs by only 1% for these compounds (2.02 Å (ref. 24 and 53) and 1.99 Å (ref. 54)). The sensitivity of the adsorption energetics to the U value for $SrIrO_3$ could indicate the challenge in using one U for every intermediate step (O*, OH*, OOH*), although, in practice, one cannot use different U for each step arbitrarily. Nevertheless, it is important to consider that each intermediate formation could lead to a different partial charge change on the surface and to a different U value, the consequence of which may include the reconstruction of the surface water layer or even the surface structure. We emphasize that U can influence the adsorption energy without significantly affecting the band structure (see ESI†). Our work suggests that the theoretical framework of electrocatalysis on transition metal oxides needs to be reconsidered for correlated systems. At the same time, our work also points to the possible utilization of the correlated effect and other many-body phenomena to break away from the scaling relations that limit the electrocatalytic activities in metallic systems.[8] Lastly, we point out that the OER electrocatalysis may also occur *via* different OER mechanisms.[49,50,55] Many alternative OER pathways have been proposed on transition metal oxides, including the seminal 3d oxo-perovskite work by Bockris and Otagawa[49] and the electrochemically deposited nickel catalysts by Nocera and co-workers.[50] We believe that obtaining correctly both the OER mechanism (*via in situ* spectroscopy) and the surface energetics will be essential for our future understanding of OER electrocatalysis.

In conclusion, we report the OER electrocatalytic activity on a $SrIrO_3(100)_p$ film grown on a $DyScO_3(110)$ substrate using MBE. We find that $SrIrO_3$ exhibits more than an order of magnitude activity higher than IrO_2 despite having the same nominal valency (Ir^{4+}). Our DFT calculations reveal that the O*, OH*, OOH* intermediate energies on $SrIrO_3$ depend sensitively on the Coulomb interaction. The sensitivity on U makes the process of assigning the intermediate energies on $SrIrO_3$ not straightforward. We therefore cannot rationalize the increased OER activity using the framework of thermodynamics-potential-limiting step. Future work in understanding the increased OER activity, along with the spectroscopic measurement of the OER mechanism will be essential to understand the OER activity on $SrIrO_3$. To our knowledge, this is the first reported OER activity of $SrIrO_3$, demonstrating that the electrocatalytic activity of the same cation valency (Ir^{4+}) in the same octahedra depends on more than the structure of the oxygen coordination environment. We propose that this may stem from the role of electronic correlations in $SrIrO_3$, which should be thoroughly examined in order to understand and potentially exploit electronic correlations for future oxide electrocatalysts.

Acknowledgements

We thank C. J. Eom for the AFM, G. McElwee for the ICP-MS measurement, and N. B. Halck, J. Rossmeisl, and R. Frydendal for insightful discussions. Support for this work is provided by the Cornell Center for Materials Research under (National Science Foundation) Grant DMR-1120296, part of the NSF MRSEC Program, the Air Force Office of Scientific Research (Grants No. FA9550-12-1-0335 and FA9550-11-1-033), and

a Research Corporation Cottrell Scholars Awards (20025). J. K. acknowledges support from the Kavli Institute at Cornell for Nanoscience Science. This work was performed in part at the Cornell NanoScale Facility (CNF), a member of the National Nanotechnology Infrastructure Network, which is supported by the National Science Foundation (Grant ECCS-1542081). G.-M. R. and G. P. acknowledge support from the Fédération Wallonie-Bruxelles through the Concerted Research Action ARC BATTAB (Convention 14/19-057). G.-M. R. is grateful to the F.R.S.-FNRS for financial support. We acknowledge access to various computational resources: the Tier-1 supercomputer of the Fédération Wallonie-Bruxelles funded by the Walloon Region (grant agreement N° 1117545), and all the facilities provided by the Université Catholique de Louvain (CISM/UCL) and by the Consortium des Équipements de Calcul Intensif en Fédération Wallonie-Bruxelles (CÉCI).

References

1 J. Greeley and N. M. Markovic, *Energy Environ. Sci.*, 2012, **5**, 9246–9256.
2 T. R. Cook, D. K. Dogutan, S. Y. Reece, Y. Surendranath, T. S. Teets and D. G. Nocera, *Chem. Rev.*, 2010, **110**, 6474–6502.
3 W. T. Hong, M. Risch, K. A. Stoerzinger, A. Grimaud, J. Suntivich and Y. Shao-Horn, *Energy Environ. Sci.*, 2015, **8**, 1404–1427.
4 R. Cao, J. S. Lee, M. L. Liu and J. Cho, *Adv. Energy Mater.*, 2012, **2**, 816–829.
5 Y. Y. Shao, S. Park, J. Xiao, J. G. Zhang, Y. Wang and J. Liu, *ACS Catal.*, 2012, **2**, 844–857.
6 S. H. Oh and L. F. Nazar, *Adv. Energy Mater.*, 2012, **2**, 903–910.
7 S. Trasatti, *J. Electroanal. Chem.*, 1980, **111**, 125–131.
8 I. C. Man, H. Y. Su, F. Calle-Vallejo, H. A. Hansen, J. I. Martinez, N. G. Inoglu, J. Kitchin, T. F. Jaramillo, J. K. Norskov and J. Rossmeisl, *ChemCatChem*, 2011, **3**, 1159–1165.
9 J. Rossmeisl, Z. W. Qu, H. Zhu, G. J. Kroes and J. K. Norskov, *J. Electroanal. Chem.*, 2007, **607**, 83–89.
10 M. T. M. Koper, *J. Electroanal. Chem.*, 2011, **660**, 254–260.
11 J. Suntivich, K. J. May, J. B. Goodenough, H. A. Gasteiger and Y. Shao-Horn, *Science*, 2011, **334**, 1383–1385.
12 L. Trotochaud, J. K. Ranney, K. N. Williams and S. W. Boettcher, *J. Am. Chem. Soc.*, 2012, **134**, 17253–17261.
13 S. Klaus, Y. Cai, M. W. Louie, L. Trotochaud and A. T. Bell, *J. Phys. Chem. C*, 2015, **119**, 7243–7254.
14 A. Grimaud, K. J. May, C. E. Carlton, Y. L. Lee, M. Risch, W. T. Hong, J. G. Zhou and Y. Shao-Horn, *Nat. Commun.*, 2013, **4**, 2439.
15 S. W. Lee, C. Carlton, M. Risch, Y. Surendranath, S. Chen, S. Furutsuki, A. Yamada, D. G. Nocera and Y. Shao-Horn, *J. Am. Chem. Soc.*, 2012, **134**, 16959–16962.
16 Y. Y. Liang, Y. G. Li, H. L. Wang and H. J. Dai, *J. Am. Chem. Soc.*, 2013, **135**, 2013–2036.
17 M. Gong, Y. G. Li, H. L. Wang, Y. Y. Liang, J. Z. Wu, J. G. Zhou, J. Wang, T. Regier, F. Wei and H. J. Dai, *J. Am. Chem. Soc.*, 2013, **135**, 8452–8455.
18 Y. Gorlin, C. J. Chung, J. D. Benck, D. Nordlund, L. Seitz, T. C. Weng, D. Sokaras, B. M. Clemens and T. F. Jaramillo, *J. Am. Chem. Soc.*, 2014, **136**, 4920–4926.
19 R. Mohamed, X. Cheng, E. Fabbri, P. Levecque, R. Kotz, O. Conrad and T. J. Schmidt, *J. Electrochem. Soc.*, 2015, **162**, F579–F586.
20 K. A. Stoerzinger, L. Qiao, M. D. Biegalski and Y. Shao-Horn, *J. Phys. Chem. Lett.*, 2014, **5**, 1636–1641.
21 T. Hepel, F. H. Pollak and W. E. O'Grady, *J. Electrochem. Soc.*, 1985, **132**, 2385–2390.
22 D. Xiao, W. G. Zhu, Y. Ran, N. Nagaosa and S. Okamoto, *Nat. Commun.*, 2011, **2**, 596.
23 S. J. Moon, H. Jin, K. W. Kim, W. S. Choi, Y. S. Lee, J. Yu, G. Cao, A. Sumi, H. Funakubo, C. Bernhard and T. W. Noh, *Phys. Rev. Lett.*, 2008, **101**, 226402.
24 J. G. Zhao, L. X. Yang, Y. Yu, F. Y. Li, R. C. Yu, Z. Fang, L. C. Chen and C. Q. Jin, *J. Appl. Phys.*, 2008, **103**, 103706.
25 J. M. Longo, J. A. Kafalas and R. J. Arnott, *J. Solid State Chem.*, 1971, **3**, 174–179.
26 D. G. Schlom, L. Q. Chen, X. Q. Pan, A. Schmehl and M. A. Zurbuchen, *J. Am. Ceram. Soc.*, 2008, **91**, 2429–2454.
27 Y. F. Nie, P. D. C. King, C. H. Kim, M. Uchida, H. I. Wei, B. D. Faeth, J. P. Ruf, J. P. C. Ruff, L. Xie, X. Pan, C. J. Fennie, D. G. Schlom and K. M. Shen, *Phys. Rev. Lett.*, 2015, **114**, 016401.
28 S. K. Panda, S. Bhowal, A. Delin, O. Eriksson and I. Dasgupta, *Phys. Rev. B: Condens. Matter Mater. Phys.*, 2014, **89**, 155102.
29 W. D. Ryden, A. W. Lawson and C. C. Sartain, *Phys. Lett. A*, 1968, **26**, 209–210.
30 J. J. Lin, S. M. Huang, Y. H. Lin, T. C. Lee, H. Liu, X. X. Zhang, R. S. Chen and Y. S. Huang, *J. Phys.: Condens. Matter*, 2004, **16**, 8035.
31 P. F. Smith, C. Kaplan, J. E. Sheats, D. M. Robinson, N. S. McCool, N. Mezle and G. C. Dismukes, *Inorg. Chem.*, 2014, **53**, 2113–2121.
32 D. M. Robinson, Y. B. Go, M. Mui, G. Gardner, Z. J. Zhang, D. Mastrogiovanni, E. Garfunkel, J. Li, M. Greenblatt and G. C. Dismukes, *J. Am. Chem. Soc.*, 2013, **135**, 3494–3501.
33 M. Garcia-Mota, M. Bajdich, V. Viswanathan, A. Vojvodic, A. T. Bell and J. K. Norskov, *J. Phys. Chem. C*, 2012, **116**, 21077–21082.
34 Z. Xu, J. Rossmeisl and J. R. Kitchin, *J. Phys. Chem. C*, 2015, **119**, 4827–4833.
35 F. Calle-Vallejo, N. G. Inoglu, H. Y. Su, J. I. Martinez, I. C. Man, M. T. M. Koper, J. R. Kitchin and J. Rossmeisl, *Chem. Sci.*, 2013, **4**, 1245–1249.
36 J. D. Blakemore, N. D. Schley, M. N. Kushner-Lenhoff, A. M. Winter, F. D'Souza, R. H. Crabtree and G. W. Brudvig, *Inorg. Chem.*, 2012, **51**, 7749–7763.
37 P. Steegstra, M. Busch, I. Panas and E. Ahlberg, *J. Phys. Chem. C*, 2013, **117**, 20975–20981.
38 P. Steegstra and E. Ahlberg, *Electrochim. Acta*, 2012, **76**, 26–33.
39 Y. X. Zhao, N. M. Vargas-Barbosa, E. A. Hernandez-Pagan and T. E. Mallouk, *Small*, 2011, **7**, 2087–2093.
40 M. E. G. Lyons and S. Floquet, *Phys. Chem. Chem. Phys.*, 2011, **13**, 5314–5335.

41 K. J. May, C. E. Carlton, K. A. Stoerzinger, M. Risch, J. Suntivich, Y. L. Lee, A. Grimaud and Y. Shao-Horn, *J. Phys. Chem. Lett.*, 2012, **3**, 3264–3270.
42 J. Suntivich, E. E. Perry, H. A. Gasteiger and Y. Shao-Horn, *Electrocatalysis*, 2013, **4**, 49–55.
43 D. Strmcnik, K. Kodama, D. van der Vliet, J. Greeley, V. R. Stamenkovic and N. M. Markovic, *Nat. Chem.*, 2009, **1**, 466–472.
44 R. Gisbert, G. Garcia and M. T. M. Koper, *Electrochim. Acta*, 2010, **55**, 7961–7968.
45 M. J. T. C. van der Niet, N. Garcia-Araez, J. Hernandez, J. M. Feliu and M. T. M. Koper, *Catal. Today*, 2013, **202**, 105–113.
46 W. Sheng, Z. Zhuang, M. Gao, J. Zheng, J. G. Chen and Y. Yan, *Nat. Commun.*, 2015, **6**, 5848.
47 K. A. Stoerzinger, M. Risch, J. Suntivich, W. M. Lu, J. Zhou, M. D. Biegalski, H. M. Christen, Ariando, T. Venkatesan and Y. Shao-Horn, *Energy Environ. Sci.*, 2013, **6**, 1582–1588.
48 Y. Lee, J. Suntivich, K. J. May, E. E. Perry and Y. Shao-Horn, *J. Phys. Chem. Lett.*, 2012, **3**, 399–404.
49 J. O. Bockris and T. Otagawa, *J. Electrochem. Soc.*, 1984, **131**, 290–302.
50 D. K. Bediako, Y. Surendranath and D. G. Nocera, *J. Am. Chem. Soc.*, 2013, **135**, 3662–3674.
51 B. Himmetoglu, A. Floris, S. de Gironcoli and M. Cococcioni, *Int. J. Quantum Chem.*, 2014, **114**, 14–49.
52 L. Wang, T. Maxisch and G. Ceder, *Phys. Rev. B: Condens. Matter Mater. Phys.*, 2006, **73**, 195107.
53 J. H. Choy, D. K. Kim, S. H. Hwang, G. Demazeau and D. Y. Jung, *J. Am. Chem. Soc.*, 1995, **117**, 8557–8566.
54 A. A. Bolzan, C. Fong, B. J. Kennedy and C. J. Howard, *Acta Crystallogr., Sect. B: Struct. Sci.*, 1997, **53**, 373–380.
55 N. B. Halck, V. Petrykin, P. Krtil and J. Rossmeisl, *Phys. Chem. Chem. Phys.*, 2014, **16**, 13682–13688.

